

Apply Non-Hermitian Physics to Realize Ultra-High-Quality Factors of Optically Trapped Particles

Yang Li¹ and Xiao Li^{1,2*}

¹Department of Physics, Southern University of Science and Technology,
Shenzhen, Guangdong 518055, China

²Department of Physics, The Hong Kong University of Science and Technology,
Hong Kong, China

*E-mail:

Xiao Li: lixiao@ust.hk

Jack Ng: wuzh3@sustech.edu.cn

Abstract

Optical trapping and binding systems are non-Hermitian. On one hand, the optical force is non-Hermitian and may pump energy into the trapped particle when the non-Hermiticity is sufficiently large. On the other hand, the ambient damping constitutes a loss to the particle. Here, we show that in a low-friction environment, the interplay between the energy pumped-in by light and the ambient dissipation can give rise to either instability or a periodic vibration characterized by a finite quality factor (Q-factor). Through a comprehensive exploration, we analyze the influence of various parameters on the non-Hermitian force field. Our investigation reveals several strategies for enhancing the non-Hermitian force field, such as augmenting particle radius and refractive index, utilizing triangular lattice optical clusters, and reducing lattice constants.

Introduction

Vibrations are almost always accompanied by dissipative damping. In principle, damping can be compensated by gain, but in most system, it is more easily said than done. We consider optical trapping and binding, where a particle is confined in vacuum, air, or water. The vibrational modes of such system are subjected to ambient damping, as consequence, finite Q-factors are expected. Recently, the non-Hermitian characteristics of optical trapping and binding systems are considered [1]. It is found that by driving the system beyond exceptional point, either by increasing the nonconservative force or increasing the number of particles, light can pump energy into the system, effectively serving as a gain. Here, we show that such non-Hermitian gain can indeed compensate the ambient damping in a low-pressure environment, significantly increases the life-time, or Q-factor, of the modes.

Optical micromanipulation is a sophisticated technique that utilizes optical forces to trap [2-5], accelerate [6-11], and pull [12-15] micro- or nano-particles. The single most widely employed tool for optical micromanipulation is the optical tweezers [16-18], which employs a tightly focused laser beam to trap a small particle near the focal point, enabling precise, contact-less, and non-invasive manipulation. Another technique, optical binding [19], proposed by Burns et al. in 1989, allows for the binding of multiple particles to create a stable lattice structure known as optical clusters [1, 20, 21] or optical matter [22-24]. Optical binding plays a crucial role in fields such as colloidal science [21, 25], nanotechnology, [23, 26, 27] and alike [28]. We shall see that the “non-Hermitian gain” work for both optical trapping and binding in a low-pressure environment.

Aqueous environments have strong dissipation that dominates over many other interactions including the non-Hermitian gain. In contrast, optical manipulation in vacuum offers some unique advantage due to its low dissipation, for example, nano-rotors in optical trapping systems can be accelerated to frequencies beyond a GHz [29, 30], making them the fastest artificial rotors developed to date. Additionally, the unique high quality factor (Q-factor) of the vacuum environment enables the detection of weak forces and torques [29, 31-33] and facilitates the observation of macroscopic quantum effects [34-36]. Optical binding can also be used to manipulate multiple particles and create ultrafast multibody oscillators [37]. These properties make optical micromanipulation in vacuum a promising tool for ultra-sensitive sensors in high-precision measurement [38, 39].

In this study, instead of reducing ambient damping (energy loss), we utilize the non-Hermiticity of optical trapping or binding to introduce energy gain into particle manipulation and balance the energy loss induced by the unavoidable ambient damping. Optical micromanipulation is

non-Hermitian due to its openness. Despite this non-Hermitian nature, most of the earlier theoretical studies focused only on conservative forces and ignored nonconservative forces. It is worth noting that recent studies [40, 41] have shown the importance of non-Hermitian properties in the stability of trapped or bound particles, with exceptional points (EPs) also being observed [1]. EP emerges with increasing non-Hermiticity. Before the emergence of EPs (low Hermiticity), the natural vibration frequencies and the corresponding eigenvectors are numbers. However, after EPs emerge (high non-Hermiticity), a pair of natural vibration frequencies join together to become conjugate pair of complex numbers, simultaneously transforming the corresponding modes into unstable complex modes. In non-Hermitian optical trapping or binding, the stability of trapped particles is determined by the competition between ambient damping and the non-Hermitian force field [3, 4, 7, 15]. The latter pumps energy into the system, allowing the particle to get further away, while the former dissipates the kinetic energy to keep the particle localized. Here, the particles lose stability when non-Hermiticity is dominant, and vice versa.

One of the most distinguishing features of the vacuum trapping system is the ultra-high mechanical Q-factor [29, 37, 42]. Here, we propose achieving a very large Q-factor by utilizing non-Hermiticity, which brings energy gain, in optical trapping or binding to balance the energy loss induced by ambient damping. We first examine a single particle trapped by Gaussian beams with different polarizations, and then we study a collection of particles optically bound by several plane waves. We demonstrate that both the optical trapping and binding systems can theoretically achieve an ultra-high Q-factor. Our study exhibits that the non-Hermiticity can be increased in optical binding systems by varying certain parameters, such as assembling triangular lattices and increasing the refractive index and particle radius. The non-Hermiticity of an optical cluster can be characterized by comparing its nonconservative and conservative contributions, which will be presented with respect to different parameters.

Results and discussion:

The time-averaged optical force is calculated using by

$$F = \oint \hat{T} \cdot dS, \quad (1)$$

where $\hat{T} = \frac{1}{2}\varepsilon_0 EE^* + \frac{1}{2}\mu_0 HH^* - \frac{1}{4}\varepsilon_0 E \cdot E^* \hat{I} - \frac{1}{4}\mu_0 H \cdot H^* \hat{I}$ is the time-averaged Maxwell stress tensor, with E and H the total electromagnetic fields. Here, ε_0 and μ_0 are the permittivity and permeability in free space, respectively. We consider a collection of spherical particles, whose electromagnetic fields can be obtained using the multi-particle Mie scattering theory [20]. N particles are trapped by optical forces at an equilibrium configuration, where the force is $\mathbf{0}$. For simplicity, we take the equilibrium configuration to be $x = 0$. The optical force field $F(x) = (F_{x,1}, F_{y,1}, F_{z,1}, \dots, F_{x,N}, F_{y,N}, F_{z,N})$ can be linearly approximated as $F(x) = \hat{K} \cdot x$, where $x = (x_1, y_1, z_1, \dots, x_N, y_N, z_N)$ represents the displacement of the particles and \hat{K} denotes the force constant matrix, with $K_{ij} = \frac{\partial F_i}{\partial x_j}$ [1, 3, 20]. Here, F_i and x_j denote the i -th and j -th components of F and x , respectively. \hat{K} is Hermitian if $\hat{K}^\dagger = \hat{K}$. However, due to the openness of optical trapping and binding system, non-Hermitian \hat{K} , characterized by $\hat{K}^\dagger \neq \hat{K}$, is commonly observed. It is worth noting that, according to Lyapunov's theorem [43], a nonlinear dynamical system is stable if and only if its linear approximation ($F(x) = \hat{K} \cdot x$) is stable. Thus the linear system we consider fully dictates the stability of the particle.

If one ignores the Brownian fluctuation, which is small at high laser power, the motion of the particles is governed by

$$m \frac{d^2 x}{dt^2} = \hat{K} \cdot x - \gamma \frac{dx}{dt}, \quad (2)$$

where m is the mass of a single particle and $\gamma = m\Gamma_0$ is the damping coefficient, with Γ_0 being inversely proportional to the environmental pressure P [44-46]. The damping rate Γ_0 is defined by [47]:

$$\Gamma_0 = \frac{6\pi\eta r}{m} \frac{0.619}{0.619 + \bar{K}n} (1 + c_K), \quad (3)$$

where η is the viscosity of the air, $Kn = \frac{\lambda_{mfp}}{r}$ is the Knudsen number, $\lambda_{mfp} = \frac{68 \times 10^{-9} P_{atm}}{P}$ is the mean free path of air, and $c_k = \frac{0.31 Kn}{(0.785 + 1.152 Kn + Kn^2)}$. One can diagonalize \acute{K} in Eq. (2) to obtain the equation for the decoupled i -th mode:

$$m \frac{d^2 q_i}{dt^2} = K_i \cdot q_i - \gamma \frac{dq_i}{dt}, \quad (4)$$

where K_i is the i -th eigenvalue of \acute{K} , and q_i is the i -th component of the generalized coordinate $q = \acute{V}^{-1}x$. Here, the columns of \acute{V} are the right-eigenvectors of \acute{K} , and one can diagonalize \acute{K} with $\acute{V}^{-1}\acute{K}\acute{V}$. By substituting the particular solution $q_i = q_{i0}e^{-i\omega_i t}$ into Eq. (4), one obtains the vibration frequency for the i -th mode:

$$\begin{aligned} \omega_{i,+} &= \frac{-i\gamma}{2m} + \sqrt{\frac{-K_i}{m} - \left(\frac{\gamma}{2m}\right)^2}, \\ \omega_{i,-} &= \frac{-i\gamma}{2m} - \sqrt{\frac{-K_i}{m} - \left(\frac{\gamma}{2m}\right)^2}. \end{aligned} \quad (5)$$

Here, we adopt a simplified approach by considering vibration frequencies as $\omega_i = \omega_{i,+}$ within a low-pressure range of 0.1-20 Torr, alongside the corresponding Q factor $Q_i = Q_{i,+}$, because the Q factor defined by $\omega_{i,\pm}$ or $\omega_{i,-}$ is the same for any real K_i when $\left(\frac{\gamma}{2m}\right)^2 < \frac{-K_i}{m}$ or any complex K_i [see Supplementary Materials].

The stability of the particles is essentially determined by $\Im[\omega_i]$, where the time dependence of the mode $q_i = q_{i0}e^{-i\omega_i t}$ diverges if $\Im[\omega_i] > 0$, and vice versa. In between, one will find a point where $\Im[\omega_i]$ is exactly 0. In this case, the mode is a neutral mode. Since it is non-decaying, in this paper, we say that it has a Q-factor of infinity, because [48]: $Q_i = \frac{-\Re[\omega_i]}{2\Im[\omega_i]}$. In a perfect vacuum characterized by $\gamma = 0$, Q_i can also be infinitely large if K_i is real and negative. However, a perfect vacuum is impossible in an experiment. Here, we utilize the complex K_i induced from non-Hermiticity (which serve as an effective gain), to compensated the inevitable dissipative losses from the ambient and realize a large Q-factor.

For optical trapping, as depicted in Fig. 1, a single ($N=1$) silica particle with a radius of 0.5 μm and a refractive index of 1.45 is trapped at the equilibrium position ($\mathbf{x}=\mathbf{0}$). This trapping is achieved by two counter-propagating Gaussian beams in the z -direction, each with a power of 1 mW. Due to the mirror symmetry of the system along the z -direction, the trapping stiffness in the z -axis is independent of the transverse xy -motion [1]. Consequently, we consider a 2-dimensional (2D) force constant matrix, denoted as $\acute{K}_{2D} = \begin{pmatrix} k_{xx} & k_{xy} \\ k_{yx} & k_{yy} \end{pmatrix}$, to describe the trapping forces on the transverse plane. All matrix can be split into a symmetric and anti-symmetric part. By selecting an appropriate coordinate system that diagonalize the symmetric part of \acute{K}_{2D} one arrives at:

$$\acute{K}'_{2D} = \begin{pmatrix} a+b & g \\ -g & a-b \end{pmatrix}. \quad (6)$$

The diagonal elements, $a+b$, and $a-b$, represent the trapping stiffness along the x - and y -directions, respectively, indicating a two-level distribution in the frequency spectrum. Here, a represents the averaged trapping stiffness, and b represents the half-level spacing between the two vibration frequency levels. In this setup, the off-diagonal element g arises from the conversion of orbital angular momentum from the spin angular momentum during beam focusing [1, 49]. It signifies the non-Hermitian coupling between the trapping stiffness in the x - and y -directions. The eigenvalues of \acute{K}'_{2D} can be analytically solved as:

$$K_{i=1,2} = a \pm \sqrt{b^2 - g^2}. \quad (7)$$

In this expression, an exceptional point (EP) is observed when $\nabla b \nabla = \nabla g \nabla$.

By manipulating the polarization ($\hat{p} = \hat{x} \cos(\xi) + i\hat{y} \sin(\xi)$) of the input beam, ranging from linear ($\xi = 0^\circ$, Fig. 1a) to circular ($\xi = 45^\circ$, Fig. 1b), the corresponding force constant matrix \acute{K}_{2D} varies with ξ . Specifically, as ξ changes from 0° to 45° [1], $\nabla b \nabla$ decreases to 0 while $\nabla g \nabla$ increases from 0. Therefore, $\nabla b \nabla = \nabla g \nabla$ is guaranteed to occur at a certain ξ , giving rise to the emergence of an exceptional point (EP). In Fig. 1(c), the natural vibration frequencies

$\omega_i = \sqrt{\frac{-K_i}{m}}$ for a particle being trapped in a 2D space are depicted as the polarization varies, where the ambient damping is neglected. Notably, an EP (green cross) is observed at $\xi \approx 18^\circ$. On the left-hand side of the EP, the frequencies ω_i are purely real, signifying stable particle trapping and an ultra-high Q-factor ($Q_i \rightarrow +\infty$) in an ideal vacuum. However, on the right-hand side of the EP, the frequencies ω_i become complex conjugates, with one of the $\Im[\omega_i]$ values being positive. Consequently, the corresponding vibration mode becomes unstable as the time evolution factor of the vibration amplitude, $e^{-i(\Re[\omega_i] + i\Im[\omega_i])t} = e^{\Im[\omega_i]t}e^{-i\Re[\omega_i]t}$, diverges over time due to the positive $\Im[\omega_i]$.

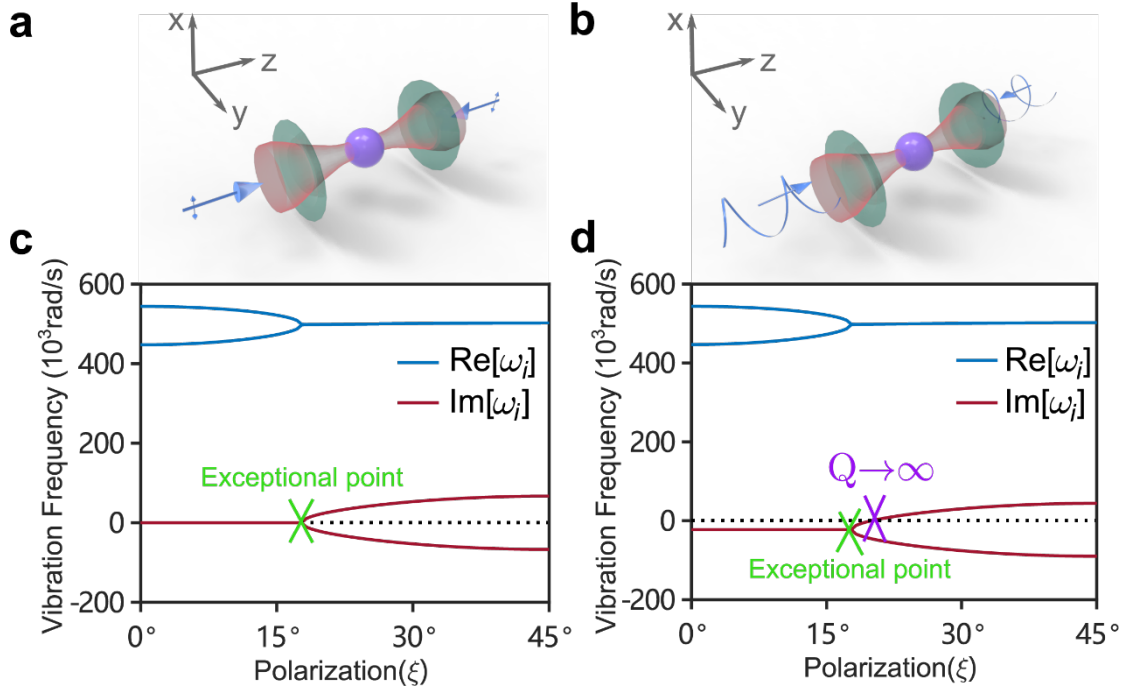


Figure 1 | The vibrational frequencies of an optically trapped silica particle (with a radius of $r = 0.5 \mu\text{m}$ and refractive index $n = 1.45$) in a vacuum are investigated as the polarization ($\hat{p} = \hat{x}\cos\xi + i\hat{y}\sin\xi$) of the counter-propagating incident Gaussian beams varies from linear ($\xi = 0^\circ$, **a**) to circular ($\xi = 45^\circ$, **b**) polarization. The incident beams, with a wavelength of $\lambda = 1.064 \mu\text{m}$, are focused by an objective lens with a numerical aperture (NA) of 0.9. Each focused beam has a power of 1 mW. The real (blue lines) and imaginary (red lines) vibrational frequencies in the x - y plane are plotted for the particle trapped in a perfect vacuum at 0 Torr pressure (see **(c)**), as well as in a low vacuum at 10 Torr pressure (see **(d)**). The exceptional points, indicated by the green cross in **(c)**, mark specific conditions where the system behavior undergoes a significant change. When the imaginary part of a vibrational frequencies exceeds 0, the particle loses stability. Additionally, the quality factor ($Q_i = \frac{-\Re[\omega_i]}{2\Im[\omega_i]}$) for the vibrational particle approaches infinity ($+\infty$), as denoted by the purple cross in **(d)**, when $\Im[\omega_i] \rightarrow 0$.

However, ambient damping is inevitable even in a vacuum trapping system and it plays a crucial role in stabilizing the optically trapped particle, when complex K_i emerges. $\Re[\omega_i]$ and $\Im[\omega_i]$, at a pressure of 10 Torr, are represented by the blue and red lines in Fig. 1(**d**), respectively. $\Im[\omega_i]$ slightly shifts downwards, resulting in $\Im[\omega_i] = 0$ occurring at $\xi \approx 20^\circ$, indicated by a purple cross, where $Q \rightarrow \infty$. On the left-hand side of the purple cross, $\Im[\omega_i] < 0$ for all i , indicating stable particle trapping. Moreover, it can be noted that ambient damping stabilizes the initially unstable complex K_i modes, which lie between the green (EP) and purple crosses. On the right-hand side of the purple cross, $\Im[\omega_i]$ is positive, rendering the particle unstable. However, by further increasing the ambient damping, we can envision that $\Im[\omega_i]$ will be negative for all i , resulting in particle stability for all polarizations (ξ).

In the case of optical binding in a vacuum, as depicted in Figure 2(a), seven dielectric particles are subjected to binding forces induced by three linearly polarized plane waves propagating at a specific angle in the x - y plane. Each particle has a refractive index of $n = 1.1$ and a radius of

$r = 0.1 \mu\text{m}$. The intensity (I_0) of the plane waves is uniformly set at $1 \text{ mW}/\mu\text{m}^2$. The particles are bound at the equilibrium position and form a stable triangular lattice cluster with a lattice constant $\sim \sqrt{3}\lambda/2$. The dynamics of this cluster is governed by Eq. (2). Due to the mirror symmetry along the z -direction, the motion in the xy -plane is decoupled from the motion in the z -direction. Therefore, we only focus on the dynamics within the 2D xy -plane, where the particle displacement is $x = (x_1, y_1, \dots, x_N, y_N)$ and the force matrix is a $2N \times 2N$ \hat{K} , where $N = 7$ for the case of Fig. 2(a). After solving Eq. (4), one can obtain the vibrational frequencies ω_i versus pressure (ambient damping) for each mode, as shown in Fig. 2(b) ($\Re[\omega_i]$) and Fig. 2(c) ($\Im[\omega_i]$) for the real and imaginary parts, respectively.

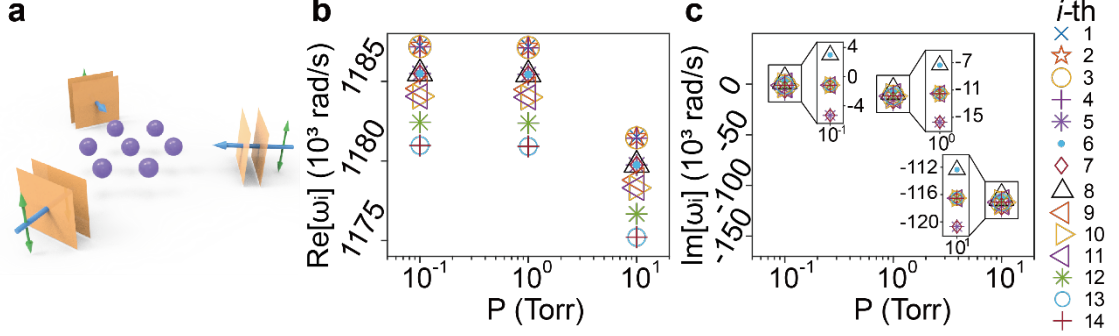


Figure 2 | Vibrational frequencies of an optically bound triangular lattice in a vacuum. (a) The cluster consists of 7 dielectric particles ($r = 0.1 \mu\text{m}$, $n = 1.1$) optically bound by 3 linearly polarized plane waves, each with an intensity (I_0) normalized to $1 \text{ mW}/\mu\text{m}^2$. As the cluster is bound in a low vacuum with a pressure (P) ranging from 0.1 to 10 Torr, the corresponding real (b) and imaginary (c) vibrational frequencies of each vibrational mode are presented. Here, the particles are considered to move within the xy -plane.

The symmetry of the lattice structure leads to the degeneracy of certain vibration modes, resulting in the overlapping vibration frequencies ($\Re[\omega_i]$) in Fig. 2(b). Additionally, the vibration modes associated with complex conjugate pairs of K_i exhibit two distinct levels of $\Im[\omega_i]$, as depicted in Fig. 2(c). According to the definition of the Q-factor, the mode with the minimum absolute value of $|\Im[\omega_i]|$ corresponds to the maximum Q-factor and is referred to as the maximum Q-factor (MQF) mode. In Figure 2(c), as the pressure (P) decreases from 1 Torr to 0.1 Torr, the $\Im[\omega_{MQF}]$ becomes positive, indicating the existence of a specific pressure level at which $\Im[\omega_{MQF}]$ equals zero, resulting in an ultra-high Q-factor ($Q \rightarrow \infty$) in optical binding systems.

According to the definition of the MQF mode, we conducted a comprehensive study on the phase diagram of MQF in optical binding. In Fig. 3(a) and 3(b), a triangular lattice ($N = 37$, lattice constant $\sim \sqrt{3}\lambda/2$) and a square lattice ($N = 36$, lattice constant $\sim \lambda$) are optically bound by three (non-standing wave) and four (standing wave) z -polarized plane waves, respectively. Different combinations of particle refractive index (n) and radius (r) were considered: $n = 1.1$, $r = 0.1 \mu\text{m}$; $n = 1.2$, $r = 0.1 \mu\text{m}$; $n = 1.1$, $r = 0.2 \mu\text{m}$; and $n = 1.2$, $r = 0.2 \mu\text{m}$. The phase diagrams of $1/Q_{MQF}$ versus the ambient pressure and plane wave intensity are shown in Fig. 3(c) and 3(d) for each combination, where the white regions indicate unstable optical binding of the particle cluster. In optical binding, non-Hermiticity is influenced not only by the particle size, refractive index, and illuminating beam intensity but also by non-standing waves, which arise due to its inherent non-Hermitian nature [1, 50]. Consequently, complex modes of \hat{K} emerge for all combinations of n and r in Fig. 3(c) when non-standing waves are present, leading to particle instability (white region) if the ambient damping is insufficient. On the other hand, in Fig. 3(d), complex modes of \hat{K} only emerge for large n and r values ($n = 1.2$, $r = 0.2 \mu\text{m}$), where the enhanced non-Hermiticity is attributed to the high refractive index and particle radius.

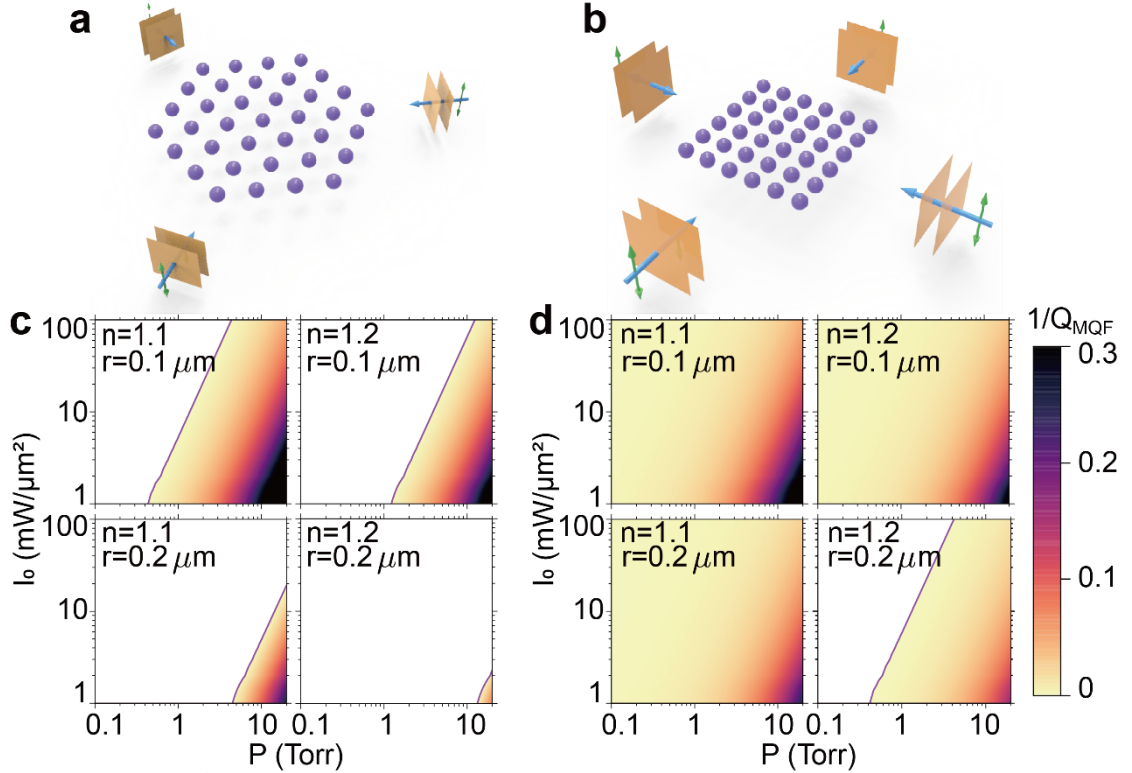


Figure 3| For optically bound clusters in a vacuum, the phase diagrams of $1/Q_{MQF}$ versus the pressure (P) in a low vacuum range (0.1-20 Torr) and the intensity (I_0) of each linearly polarized plane wave (1-100 $mW/\mu m^2$) are shown for the triangular lattice (a) and square lattice (b). Various combinations of refractive index and particle radius are considered: $n = 1.1$, $r = 0.1 \mu m$; $n = 1.2$, $r = 0.1 \mu m$; $n = 1.1$, $r = 0.2 \mu m$; and $n = 1.2$, $r = 0.2 \mu m$. In panels (c) and (d), the pink lines indicate the ultra-high Q-factors, where $1/Q_{MQF} \rightarrow 0$.

In Fig. 3(c-d), the pink lines represent the ultra-high Q-factor ($1/Q_{MQF} \rightarrow 0$), and they can be accurately fitted with the logarithmic equation:

$$\log(I_0) = a \cdot \log(P) + b. \quad (8)$$

The slope (a) of Eq. (8) for both the triangular (Fig. 3(c)) and square (Fig. 3(d)) lattice structures turns out to be a constant value of $a = 2$, which can be perfectly explained by the definition of the critical damping coefficient in optical binding. In a vacuum, the non-Hermitian optical binding system exhibits a critical pressure, characterized by a critical damping coefficient $\gamma_{critical} = \frac{\sqrt{m}|\Im(K_i)|}{\sqrt{\Re(K_i)}}$ [20]. If the ambient damping (γ) exceeds $\gamma_{critical}$, the particles remain stable; conversely, if it is less than $\gamma_{critical}$, the particles become unstable. This critical pressure (damping) corresponds to an ultra-high Q-factor, at which $\Im[\omega_{MQF}]$ becomes zero. Since the eigenvalue K_i of the force constant matrix (\dot{K}) is proportional to the intensity (I_0) of the plane wave and the ambient damping γ is proportional to the ambient pressure (P), it is demonstrated that the critical pressure ($P_{critical}$) is proportional to the square root of the intensity (I_0):

$$P_{critical} \propto \sqrt{I_0}. \quad (9)$$

By taking the logarithm of Eq. (9) and comparing it with Eq. (8), we find that the slope $a = 2$.

Given the significant impact of particle size, refractive index, and standing wave or non-standing wave on the non-Hermiticity of optically bound particles, we conducted a thorough study of the phase diagrams illustrating the relationship between the non-Hermiticity and these parameters. By decomposing \dot{K} into its symmetric (\dot{S}) and antisymmetric (\dot{A}) components, where $\dot{S} = \frac{\dot{K} + \dot{K}^T}{2}$ characterizes the Hermitian (conservative) force field and $\dot{A} = \frac{\dot{K} - \dot{K}^T}{2}$

characterizes the non-Hermitian (nonconservative) force field, we can diagonalize \hat{S} as $\hat{S}' = \hat{\Lambda}\hat{S}\hat{\Lambda}^{-1}$, with $\hat{\Lambda}$ being the eigenvector matrix of \hat{S} . Accordingly, \hat{A} is transformed to $\hat{A}' = \hat{\Lambda}\hat{A}\hat{\Lambda}^{-1}$. We can now define a parameter called R :

$$R = \frac{\sum |A'_{ij}|}{\sum |S'_{ij}|}. \quad (10)$$

This parameter quantifies the significance of the non-Hermiticity of \hat{K} . Here, A'_{ij} and S'_{ij} are the matrix elements of \hat{A}' and \hat{S}' , respectively.

We analyze the phase diagrams of R in relation to the particle radius (r) and refractive index (n) for various lattice structures. These include triangular lattices consisting of 7 spheres (Fig. 4(**a1-a4**)) or 19 spheres (Fig. 4(**b1-b4**)), as well as square lattices with 9 spheres (Fig. 4(**c1-c4**)) or 16 spheres (Fig. 4(**d1-d4**)). We also consider different lattice constants (d) such as $d = 1.1\lambda$ (Fig. 4(**b2-d2**)), $d = 1.5\lambda$ (Fig. 4(**b3-d3**)), and $d = 2.0\lambda$ (Fig. 4(**b4-d4**)). In Figure 4, it is observed that optically bound clusters induced by non-standing waves (triangular lattice) exhibit larger values of R compared to those induced by standing waves (square lattice). The phase diagrams clearly demonstrate the significant influence of non-standing waves, which is non-Hermitian (non-conservative) by nature, on R . Increasing the values of r , n , or the number of particles (N) enhances multiple scattering, resulting in larger values of R in the phase diagrams. Conversely, increasing the lattice constant (d) weakens multiple scattering, leading to a decrease in R across the phase diagrams. The highest impact of non-Hermiticity is observed in Fig. 4(**b2**), while the lowest impact is observed in Fig. 4(**c4**). Furthermore, it is important to note that R is also influenced by the optical path difference, characterized by $2r(n-1) = \text{const}$, between the light passing through a single particle and a vacuum, as observed in the hyperbolic patterns within the phase diagrams. For instance, the hyperbolic pattern in Fig. 4(**b3**) can be accurately described by the equation $2r(n-1) = 0.7\lambda$, as indicated by the pink line in Fig. 4(**b3**).

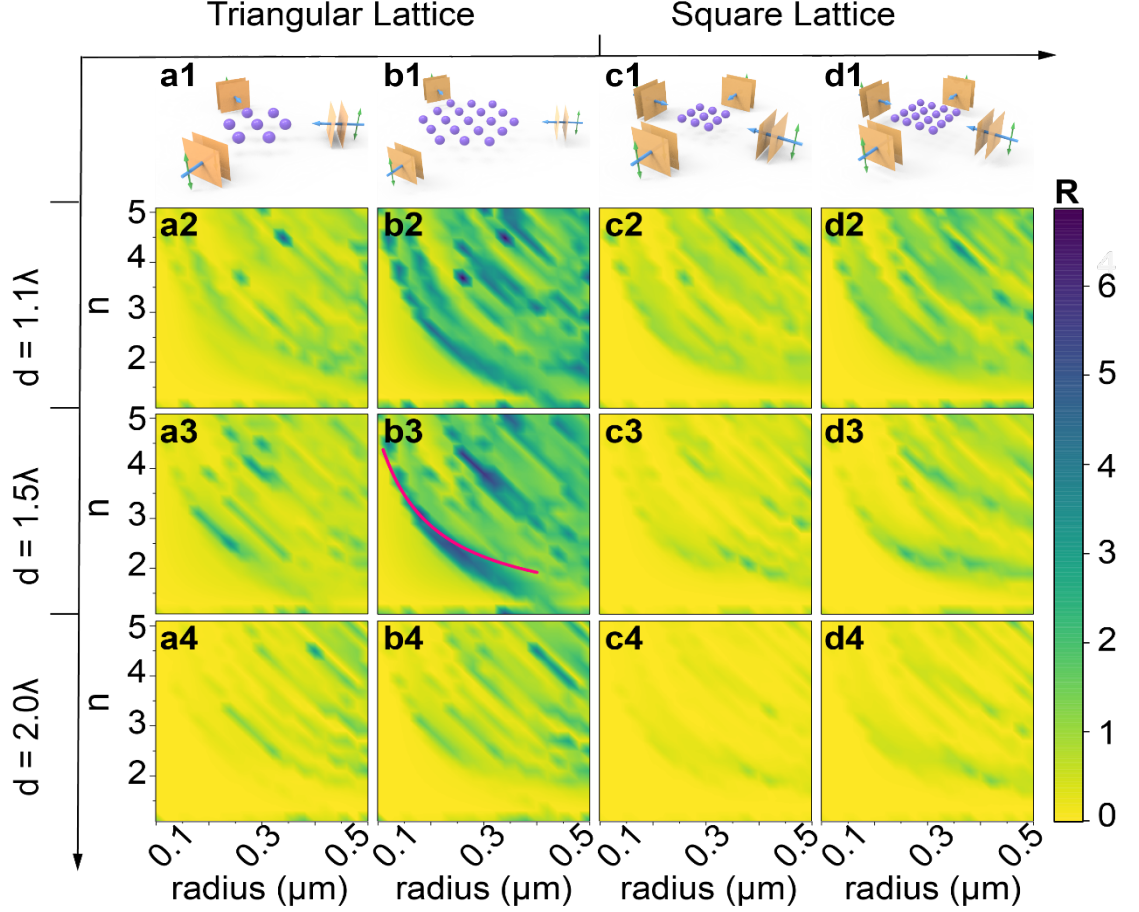


Figure 4| The phase diagrams depict the non-Hermiticity of optically bound clusters in a vacuum for triangular lattice (**a1** and **b1**) and square lattice (**c1** and **d1**), versus the radius r (from $0.1 \mu\text{m}$ to $0.5 \mu\text{m}$) and refractive index n (from $0.1 \mu\text{m}$ to $0.5 \mu\text{m}$) of the particles. The non-Hermiticity is characterized by the $R = \frac{\sum |A'_{ij}|}{\sum |S'_{ij}|}$. The phase diagrams cover various lattice structures, including a triangular lattice with 7 particles (**a2-a4**), a triangular lattice with 19 particles (**b2-b4**), a square lattice with 9 particles (**c2-c4**), and a square lattice with 16 particles (**d2-d4**). Additionally, different lattice constants are considered, namely $d = 1.1\lambda$ (**a2-d2**); $d = 1.5\lambda$ (**a3-d3**); $d = 2.0\lambda$ (**a4-d4**). The diagrams reveal distinctive hyperbolic patterns resulting from the interference structure characterized by $2r(n-1) = \text{const}$. For instance, one of the hyperbolic curves in (**b3**) can be accurately fitted with a pink line representing $2r(n-1) = 0.7\lambda$.

Conclusions

In conclusion, non-Hermitian physics is applied to achieve an ultra-high Q-factor for an optically trapped particle or an optically bound multi-particle lattice in a vacuum, accounting for the presence of ambient damping. By adjusting the non-Hermiticity or ambient damping, it becomes possible to achieve a very high Q-factor. The parameters influencing non-Hermiticity in optical binding have been comprehensively discussed and presented. These ultra-high Q-factor oscillators have significant potential in the measurement of weak forces and torques [31, 38, 39, 51], given that measurement sensitivity is inversely proportional to the Q-factor [28, 29].

Reference:

1. Li, X., et al., *Non-Hermitian physics for optical manipulation uncovers inherent instability of large clusters*. Nature Communications, 2021. **12**(1): p. 6597.
2. Ashkin, A., *History of optical trapping and manipulation of small-neutral particle, atoms, and molecules*. IEEE Journal of Selected Topics in Quantum Electronics, 2000. **6**(6): p. 841-856.
3. Ng, J., Z. Lin, and C.T. Chan, *Theory of Optical Trapping by an Optical Vortex Beam*. Physical Review Letters, 2010. **104**(10): p. 103601.
4. Li, Y., L.-M. Zhou, and N. Zhao, *Anomalous motion of a particle levitated by Laguerre-Gaussian beams*. Optics Letters, 2021. **46**(1): p. 106-109.
5. Yuanjie, Y., et al., *Optical trapping with structured light: a review*. Advanced Photonics, 2021. **3**(3): p. 034001.
6. Arita, Y., et al., *Coherent oscillations of a levitated birefringent microsphere in vacuum driven by nonconservative rotation-translation coupling*. Science Advances. **6**(23): p. eaaz9858.
7. Shao, L., et al., *Gold Nanorod Rotary Motors Driven by Resonant Light Scattering*. ACS Nano, 2015. **9**(12): p. 12542-12551.
8. Shao, L. and M. Käll, *Light-Driven Rotation of Plasmonic Nanomotors*. Advanced Functional Materials, 2018. **28**(25): p. 1706272.
9. Tang, S., et al., *Structure-Dependent Optical Modulation of Propulsion and Collective Behavior of Acoustic/Light-Driven Hybrid Microbowls*. Advanced Functional Materials, 2019. **29**(23): p. 1809003.
10. Li, Y., et al., *Plasmon-coupling-induced photon scattering torque*. Journal of the Optical Society of America B, 2022. **39**(3): p. 671-676.
11. Wu, X., et al., *Light-driven microdrones*. Nature Nanotechnology, 2022. **17**(5): p. 477-484.
12. Chen, J., et al., *Optical pulling force*. Nature Photonics, 2011. **5**(9): p. 531-534.
13. Ding, K., et al., *Realization of optical pulling forces using chirality*. Physical Review A, 2014. **89**(6): p. 063825.
14. Wang, H., et al., *Janus Magneto-Electric Nanosphere Dimers Exhibiting Unidirectional Visible Light Scattering and Strong Electromagnetic Field Enhancement*. ACS Nano, 2015. **9**(1): p. 436-448.
15. Li, X., et al., *Optical pulling at macroscopic distances*. Science Advances, 2019. **5**(3): p. eaau7814.
16. Ashkin, A., *Acceleration and Trapping of Particles by Radiation Pressure*. Physical Review Letters, 1970. **24**(4): p. 156-159.
17. Ashkin, A. and J.M. Dziedzic, *Optical levitation in high vacuum*. Applied Physics Letters, 1976. **28**(6): p. 333-335.
18. Ashkin, A., et al., *Observation of a single-beam gradient force optical trap for dielectric particles*. Optics Letters, 1986. **11**(5): p. 288-290.
19. Burns, M.M., J.-M. Fournier, and J.A. Golovchenko, *Optical binding*. Physical Review Letters, 1989. **63**(12): p. 1233-1236.
20. Ng, J., et al., *Photonic clusters formed by dielectric microspheres: Numerical simulations*. Physical Review B, 2005. **72**(8): p. 085130.
21. Nan, F., et al., *Dissipative Self-Assembly of Anisotropic Nanoparticle Chains with Combined Electrodynamic and Electrostatic Interactions*. Advanced Materials, 2018. **30**(45): p. 1803238.
22. Burns, M.M., J.-M. Fournier, and J.A. Golovchenko, *Optical Matter: Crystallization and Binding in Intense Optical Fields*. Science, 1990. **249**(4970): p. 749-754.
23. Parker, J., et al., *Optical matter machines: angular momentum conversion by collective modes in optically bound nanoparticle arrays*. Optica, 2020. **7**(10): p. 1341-1348.
24. Huang, C.-H., et al., *The primeval optical evolving matter by optical binding inside and outside the photon beam*. Nature Communications, 2022. **13**(1): p. 5325.
25. Wei, M.-T., et al., *Lateral optical binding between two colloidal particles*. Scientific Reports, 2016. **6**(1): p. 38883.
26. Tanaka, Y.Y., et al., *Plasmonic linear nanomotor using lateral optical forces*. Science Advances, 2020. **6**(45): p. eabc3726.

27. Duan, X.-Y., et al., *Transverse optical binding for a dual dipolar dielectric nanoparticle dimer*. Physical Review A, 2021. **103**(1): p. 013721.
28. Svak, V., et al., *Stochastic dynamics of optically bound matter levitated in vacuum*. Optica, 2021. **8**(2): p. 220-229.
29. Ahn, J., et al., *Ultrasensitive torque detection with an optically levitated nanorotor*. Nature Nanotechnology, 2020. **15**(2): p. 89-93.
30. Jin, Y., et al., *6 GHz hyperfast rotation of an optically levitated nanoparticle in vacuum*. Photonics Research, 2021. **9**(7): p. 1344-1350.
31. Jain, V., et al., *Direct Measurement of Photon Recoil from a Levitated Nanoparticle*. Physical Review Letters, 2016. **116**(24): p. 243601.
32. Ahn, J., et al., *Optically Levitated Nanodumbbell Torsion Balance and GHz Nanomechanical Rotor*. Physical Review Letters, 2018. **121**(3): p. 033603.
33. Nan, F. and Z. Yan, *Optical Sorting at the Single-Particle Level with Single-Nanometer Precision Using Coordinated Intensity and Phase Gradient Forces*. ACS Nano, 2020. **14**(6): p. 7602-7609.
34. Tebbenjohanns, F., et al., *Quantum control of a nanoparticle optically levitated in cryogenic free space*. Nature, 2021. **595**(7867): p. 378-382.
35. Zhang, H., X. Chen, and Z.-q. Yin, *Quantum Information Processing and Precision Measurement Using a Levitated Nanodiamond*. Advanced Quantum Technologies, 2021. **4**(8): p. 2000154.
36. Shen, K., et al., *On-chip optical levitation with a metalens in vacuum*. Optica, 2021. **8**(11): p. 1359-1362.
37. Arita, Y., E.M. Wright, and K. Dholakia, *Optical binding of two cooled micro-gyroscopes levitated in vacuum*. Optica, 2018. **5**(8): p. 910-917.
38. Ranjit, G., et al., *Zeptonewton force sensing with nanospheres in an optical lattice*. Physical Review A, 2016. **93**(5): p. 053801.
39. Shi, H., et al., *Optical binding and lateral forces on chiral particles in linearly polarized plane waves*. Physical Review A, 2020. **101**(4): p. 043808.
40. Feng, L., R. El-Ganainy, and L. Ge, *Non-Hermitian photonics based on parity-time symmetry*. Nature Photonics, 2017. **11**(12): p. 752-762.
41. Wang, H., et al., *Topological physics of non-Hermitian optics and photonics: a review*. Journal of Optics, 2021. **23**(12): p. 123001.
42. Zhou, L.-M., et al., *Optical levitation of nanodiamonds by doughnut beams in vacuum*. Laser & Photonics Reviews, 2017. **11**(2): p. 1600284.
43. Seyranian, A.P. and A.A. Mailybaev, *Multiparameter stability theory with mechanical applications*. Vol. 13. 2003: World Scientific.
44. Beresnev, S.A., V.G. Chernyak, and G.A. Fomyagin, *Motion of a spherical particle in a rarefied gas. Part 2. Drag and thermal polarization*. Journal of Fluid Mechanics, 1990. **219**: p. 405-421.
45. Li, T., S. Kheifets, and M.G. Raizen, *Millikelvin cooling of an optically trapped microsphere in vacuum*. Nature Physics, 2011. **7**(7): p. 527-530.
46. Hempston, D., et al., *Force sensing with an optically levitated charged nanoparticle*. Applied Physics Letters, 2017. **111**(13): p. 133111.
47. Gieseler, J., et al., *Subkelvin Parametric Feedback Cooling of a Laser-Trapped Nanoparticle*. Physical Review Letters, 2012. **109**(10): p. 103603.
48. Jackson, J.D., *Classical Electrodynamics*. 3rd ed. 1999: Wiley. 371-372.
49. Zhao, Y., et al., *Spin-to-Orbital Angular Momentum Conversion in a Strongly Focused Optical Beam*. Physical Review Letters, 2007. **99**(7): p. 073901.
50. Du, J., et al., *Tailoring Optical Gradient Force and Optical Scattering and Absorption Force*. Scientific Reports, 2017. **7**(1): p. 18042.
51. Metzger, N.K., et al., *Measurement of the Restoring Forces Acting on Two Optically Bound Particles from Normal Mode Correlations*. Physical Review Letters, 2007. **98**(6): p. 068102.